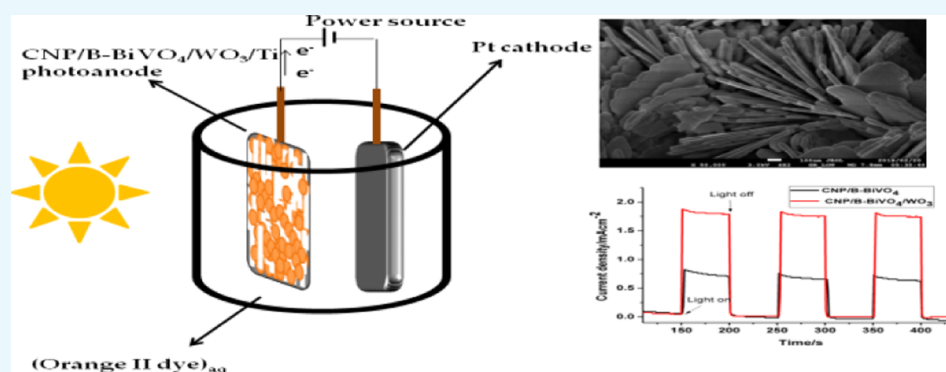Article

Solar-Light-Responsive Titanium-Sheet-Based Carbon Nanoparticles/B-BiVO₄/WO₃ Photoanode for the Photoelectrocatalytic Degradation of Orange II Dye Water Pollutant

Gbenga M. Peleyeju,[†] Eseoghene H. Umukoro,[†] Jonathan O. Babalola,[‡] and Omotayo A. Arotiba*,[†,§]

[†]Department of Chemical Sciences and [§]Centre for Nanomaterials Science Research, University of Johannesburg, Johannesburg 2028, South Africa

[‡]Department of Chemistry, University of Ibadan, Ibadan 200212, Nigeria

ABSTRACT: We report the preparation and application of a heterostructured photoelectrocatalyst comprising carbon nanoparticles (CNPs) and boron codoped BiVO₄ and WO₃ for the removal of an organic dye pollutant in water. The materials, synthesized by hydrothermal method, were characterized by X-ray diffraction, diffuse reflectance UV−visible spectroscopy, energy-dispersive X-ray spectroscopy, and electron microscopy. The catalysts were immobilized on treated titanium sheets by drop-casting. The fabricated electrodes were characterized by linear sweep voltammetry (LSV) and chronoamperometry. Diffuse reflectance spectroscopy of the catalysts reveals that the incorporation of CNPs and B into the structure of monoclinic BiVO₄ enhanced its optical absorption in both UV and visible regions. The LSV measurements carried out in 0.1 M Na₂SO₄ showed that the BiVO₄- and WO₃-based photoelectrode demonstrated significant photoactivity. CNP/B-BiVO₄ and CNP/B-BiVO4/WO₃ photoanodes gave photocurrent densities of approximately 0.83 and 1.79 mA/cm², respectively, at 1.2 V (vs 3 M Ag/AgCl). The performance of the electrodes toward degradation of orange II dye was in the order BiVO₄ < B-BiVO₄ < WO₃ < CNP-BiVO₄ < CNP/B-BiVO₄ < CNP/B-BiVO₄/WO₃, and the apparent rate constants obtained by fitting the experimental data into the Langmuir Hinshelwood kinetic model are 0.0924, 0.1812, 0.254, and 0.845 h⁻¹ for BiVO₄, WO₃, CNP/B-BiVO₄, and CNP/B-BiVO₄/WO₃, respectively. The chemical oxygen demand abatement after 3 h of electrolysis at the best performing photoanode was 58%. The study showed that BiVO₄ and WO₃ are promising anodic materials for photoelectrocatalytic water treatment plant.

1. INTRODUCTION

Photoelectrocatalytic (PEC) process has been indicated to hold promise for wastewater remediation and energy conversion.[1] In this technique, electrical energy is applied to a photocatalytic system to obtain synergistic benefit. In the last few years, combining electrochemical process and photocatalysis has been shown to yield improved performance for organic pollutant degradation compared to either electro-oxidation or photocatalysis alone. This enhanced performance has been attributed to the ability of the applied bias potential to promote the separation of the photogenerated hole and electron pairs.[2−4]

Photocatalysts that are sensitive in the visible region of the solar spectrum have received considerable attention as anodic materials for PEC[5−7] because utilizing sunlight for the process promotes sustainability. For instance, BiVO₄ and its composites have been used as photoanodes in the PEC system for hydrogen production via water splitting and organic contaminant decomposition.[8−12] Having a narrow band gap of 2.4 eV, BiVO₄ is an ideal semiconductor for visible-light-driven processes. It is nontoxic, stable to photocorrosion, inexpensive, and can be obtained via simple synthetic routes.[13] However, apart from the rapid recombination of electron−hole pairs,[14] BiVO₄ also suffers from poor electrical conductivity and low adsorptive performance.[15] These drawbacks make BiVO₄ an inefficient photocatalyst for pollutant degradation.
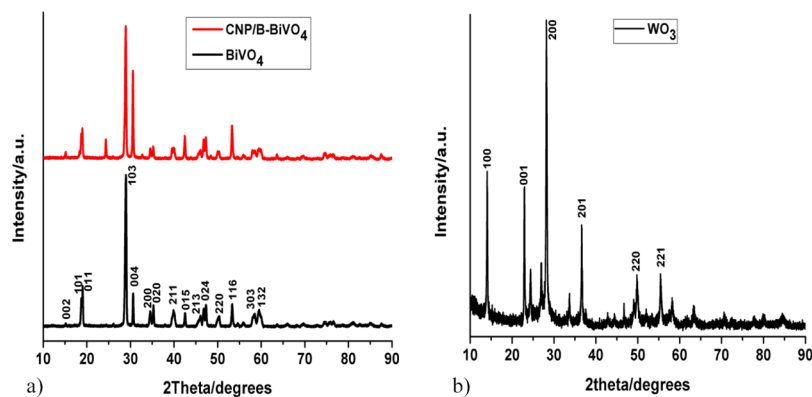
Figure 1. Powder XRD patterns of (a) BiVO$_4$ and CNP/B-BiVO$_4$ and (b) WO$_3$.

Studies have shown that the photocatalytic/PEC degradation of organic pollutants at pristine BiVO$_4$ presented low removal efficiency.[16−19]

WO$_3$ (band gap, 2.5−2.8 eV) is another promising material for PEC. It is inexpensive, demonstrates low susceptibility to photocorrosion, exhibits appreciable stability in acidic and oxidative conditions, and nontoxic.[20−22] Importantly, WO$_3$ is being explored as a potential photocatalyst for destruction of organic pollutants because of the high oxidation power of its valence-bound holes.[23] In spite of its impressive properties, the photocatalytic activity of WO$_3$ is poor owing to its relatively low conduction band edge. The position of the conduction band edge is unfavorable for one-electron reduction of adsorbed oxygen molecules.[24] This leads to accumulation of photogenerated electrons and their consequent recombination with the holes which are needed for oxidation of target compounds. As a result, improving the photocatalytic activity of WO$_3$ by modifying its electronic structure has been the focus of many studies. It has been reported that tuning the morphology/structure of WO$_3$ can yield a catalyst with enhanced charge separation and improved photoactivity.[20,25−28] Theerthagiri et al., Zhang et al., and Yao et al., in separate studies, showed that WO$_3$ nanorods possess suitable physicochemical properties for enhanced photocatalytic performance.[29−31]

Fabricating a hybrid of two or more semiconductors has been hinted as one of the plausible approaches to overcome the challenges of electron and hole recombination.[32−36] Similarly, some other limitations associated with individual photocatalyst such as the low conduction band edge in WO$_3$ and the poor charge mobility in BiVO$_4$ can also be circumvented by this approach.[3] The resulting nanocomposite catalysts have been reported to display much higher activity than the individual materials. Xia et al. reported the oxidation of phenol on a Fe$_2$O$_3$/BiVO$_4$ thin film anode via PEC process.[37] The composite photoanode demonstrated superior performance to the pristine BiVO$_4$ anode. The authors attributed the enhanced degradation performance to the ultrathin iron oxide, which minimized charge carrier recombination in BiVO$_4$. In another report by Martins et al.,[38] WO$_3$-modified TiO$_2$ nanotube array (NTA) exhibited better mineralization efficiency than the unmodified TiO$_2$ (NTAs) when both electrodes were employed for the PEC degradation of the endocrine-disrupting compound propyl paraben. Similarly, Wei et al.[39] reported that decontamination of coking wastewater containing phenolic compounds was much more efficient at heterostructured TiO$_2$/g-C$_3$N$_4$ than at

pure TiO$_2$ and g-C$_3$N$_4$. The improvement in the PEC efficiency was attributed partly to the heterojunction that is formed between the two photocatalysts which suppresses the recombination rate of electrons and holes.

In this work, BiVO$_4$ has been modified with carbon nanoparticles (CNPs) and boron to obtain a photocatalyst denoted as CNP/B-BiVO$_4$. This catalyst was then coupled to WO$_3$ nanorods and the resulting nanocomposite was immobilized on Ti plate. The photoanode, CNP/B-BiVO$_4$/WO$_3$, was then employed for the catalytic oxidation of orange II dye. A few studies have reported the use of BiVO$_4$/WO$_3$ as anodic material in PEC experiments.[32,40,41] In this study, we hypothesized that modification of BiVO$_4$ with substances such as CNP and B would impact positively on the photocatalytic performance of the semiconductor. In addition, we envisaged that coupling this modified material to WO$_3$ nanorods will provide a nanocomposite anode with desirable properties for PEC applications.

2. RESULTS AND DISCUSSION

2.1. XRD Analyses. The X-ray diffraction (XRD) patterns of the electrode materials are shown in Figure 1. The diffraction peaks in the XRD pattern of pure BiVO$_4$ (Figure 1) can be indexed to monoclinic scheelite structure of BiVO$_4$ (JCPDS card no. 14-0688).[42,43] The XRD pattern of CNPs and B codoped BiVO$_4$ shows an additional peak at 24°, which can be ascribed to the (002) plane of graphite.

The XRD pattern of WO$_3$ (Figure 1b) shows diffraction peaks at 2θ = 14.1, 22.9, 28.2, 36.5, 49.9, and 55.4°, which correspond to the (100), (001), (200), (201), (220), and (221) crystal planes, respectively, of the hexagonal structure of WO$_3$ (JCPDS card no. 75-2187).[44,45]

2.2. Morphology Investigations, EDS Analysis, and Elemental Mapping. The scanning electron microscopy (SEM) and transmission electron microscopy (TEM) images, energy-dispersive spectroscopy (EDS) spectra, and elemental maps are presented in Figures 2 and 3. From the SEM image of pristine BiVO$_4$ (Figure 2a), it can be observed that the sizes of the nanoparticles formed are largely uniform. The particles seem to be closely packed. The SEM image of the doped BiVO$_4$ (Figure 2b) shows a morphological characteristic of a composite material. It shows some plate-like structures with embedded particles and the constituents seem to be well integrated. The electron images show that the dimensions of the materials are much less than 100 nm. The elemental map (Figure 2c) confirms the presence of B in the nanocomposite, with the element uniformly distributed within the material.
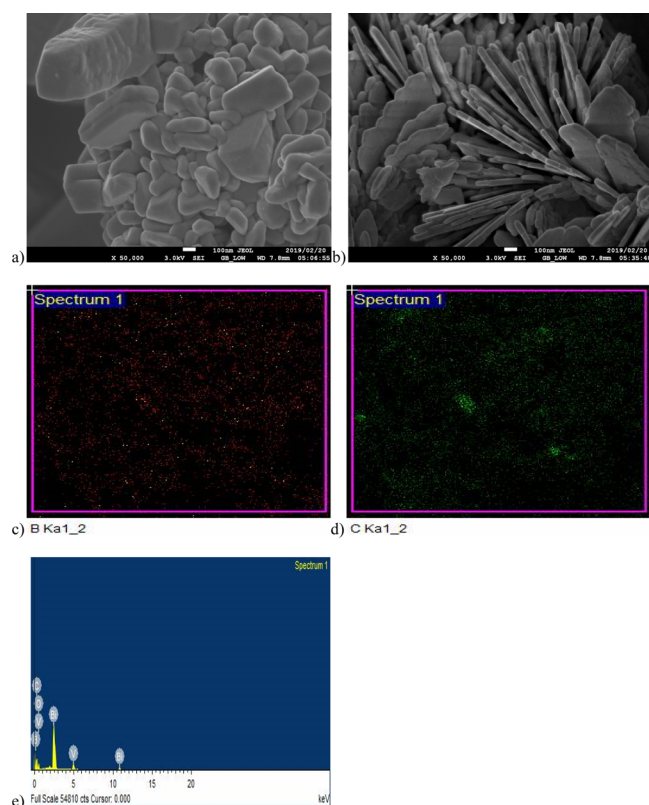
Figure 2. SEM images of (a) $BiVO_4$ and (b) $CNP/B\text{-}BiVO_4$, and elemental maps for (c) B and (d) C. (e) EDS spectrum of $CNP/B\text{-}BiVO_4$.
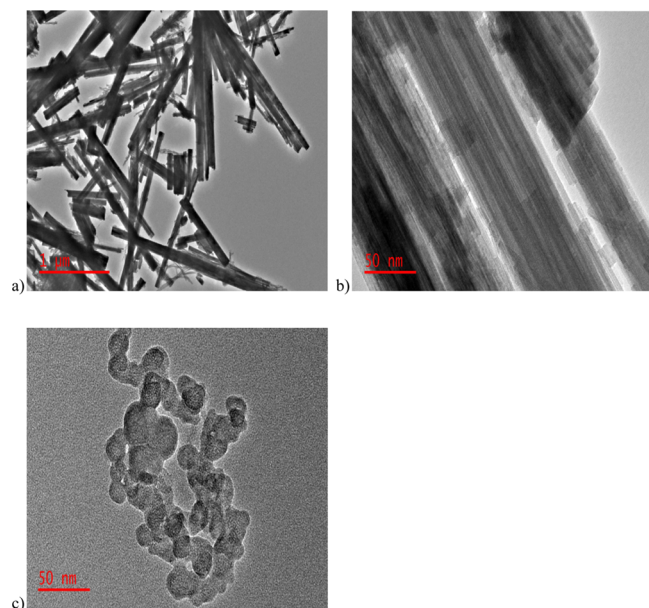

Figure 3. TEM images of (a,b) WO_3 and (c) CNP.

Similarly, Figure 2d reveals that carbon particles are present in the nanocomposite material. The EDS spectrum (Figure 2e) further confirms the presence of B, although it has a very low intensity owing to its very low concentration compared with the other elements in the composite material.

The TEM images of the synthesized WO_3 nanorods are shown in Figure 3a.b. The image at 1 μm (Figure 3a) reveals that the rods are of different lengths, but the diameter seems to

be essentially the same. The TEM image of the carbon particles is presented in Figure 3c, where the particles appear to be spherical and agglomerated.

2.3. BET Surface Area Analysis. Nitrogen adsorption— desorption experiment was performed to investigate the Brunauer–Emmett–Teller (BET) surface area of the pristine and composite materials. The adsorption isotherms of $BiVO_4$, CNP, $CNP/B\text{-}BiVO_4$, and WO_3 are given in Figure 4, and the specific BET surface areas are presented in Table 1. From the values in the table, it is obvious that incorporation of CNP into the lattices of $BiVO_4$ resulted in an increase in the surface area of the photocatalyst. Higher surface area is beneficial for interaction between the organic pollutant and the photo-electrocatalyst, and this will aid overall degradation efficiency. Similarly, the comparatively high BET surface area of WO_3 nanorods will contribute significantly to the adsorption capability of the heterojunction photoanode, which will enhance its catalytic performance.

2.4. Diffuse Reflectance Spectroscopy. Diffuse reflectance spectroscopy (DRS) is a valuable technique that can be used to gain insights into the electronic states of semiconducting materials. The UV−vis absorption spectra of $BiVO_4$, WO_3, and $CNP/B\text{-}BiVO_4$ are shown in Figure 5. The intrinsic absorption bands of both the pristine $BiVO_4$ and doped $BiVO_4$ span over the UV and visible light regions, while that of WO_3 seem to be strong within the UV region, extending slightly into the visible region. This absorption characteristic of WO_3 is in agreement with earlier reports.[46,47] The doped $BiVO_4$ demonstrates superior visible light absorption compared to the pristine $BiVO_4$. In addition, the absorption edge of the CNP and B codoped $BiVO_4$ exhibits a red shift. The extension of the absorption edge of the doped material may be as a result of band transitions occurring because of the presence of impurities in the forbidden band.[48] The band gap energies of the catalysts (Figure 6) were estimated from a plot of $(F(R) \times h\nu)^{1/2}$ against $h\nu$, where $F(R)$ is the Kubelka−Munk function given by $(1 - R)^2/2 \times R$ (R is reflectance), and $h\nu$ is the incident photon energy.[49,50]

2.5. Linear Sweep Voltammetry and Photocurrent Response. The linear sweep voltammograms of the fabricated photoanodes were obtained in the dark and in the presence of light. As shown in Figure 7a, the current responses of both $CNP/B\text{-}BiVO_4$ and $CNP/B\text{-}BiVO_4/WO_3$ in the dark are not significantly different until reaching a potential of about 1.0 V, with the $CNP/B\text{-}BiVO_4/WO_3$ electrode displaying a slightly higher current than the codoped $BiVO_4$ electrode (0.16 and 0.15 mA/cm^2 at 1.3 V). Apparently, the presence of WO_3 contributed to the current signal of the $CNP/B\text{-}BiVO_4/WO_3$ electrode. It is well known that WO_3 exhibits better charge-transfer property than $BiVO_4$.[51,52] In addition, in both doped $BiVO_4$ and heterostructured electrodes, photocurrent seems to increase as the anodic potential increases. In the presence of light, the photoanodes showed markedly higher photocurrents (1.25 and 2.20 mA/cm^2 at 1.3 V for $CNP/B\text{-}BiVO_4$ and $CNP/B\text{-}BiVO_4/WO_3$, respectively) than those recorded under dark condition (Figure 6b). The significant photocurrent enhancement recorded by the coupled semiconductor anode can be attributed to the contributions from both $BiVO_4$ and WO_3 (Figure 7b). The excellent charge transport property of WO_3 and the high visible light activity of $BiVO_4$ are beneficial for improved photoactivity. As evident in Figure 7b, the photocurrent responses at both $CNP/B\text{-}BiVO_4$ and $CNP/B\text{-}BiVO_4/WO_3$ are stable over the time range shown.
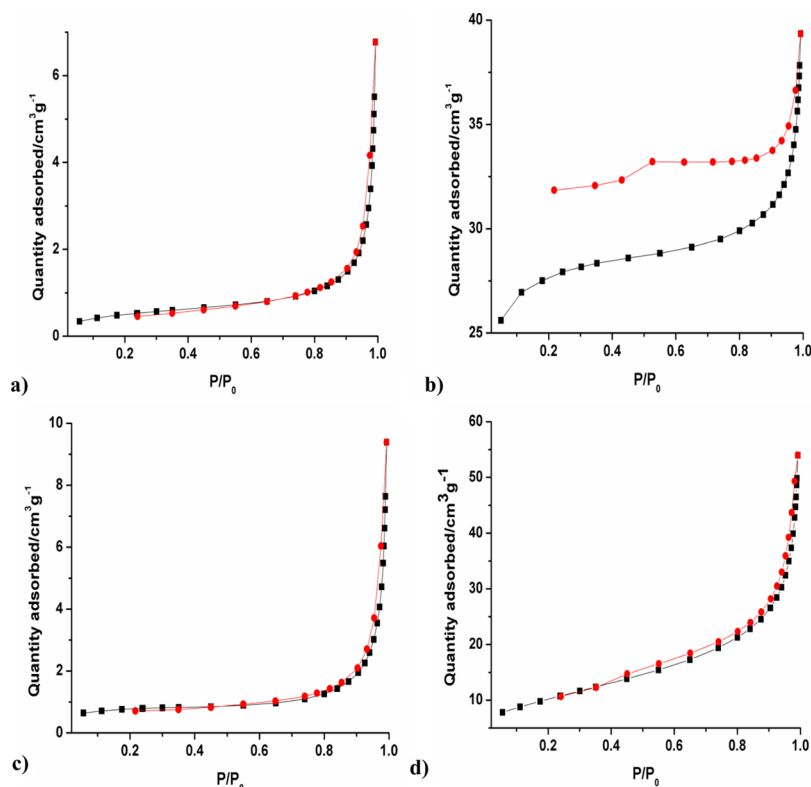
Figure 4. Nitrogen adsorption−desorption isotherms of (a) pristine $BiVO_4$, (b) CNP, (c) CNP/B-$BiVO_4$, and (d) WO_3.

Table 1. BET Surface Area of Pristine $BiVO_4$, CNP, Doped $BiVO_4$, and WO_3

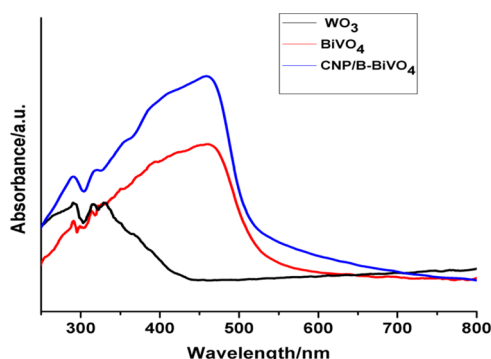| sample	BET surface area/$m^2 \ g^{-1}$
$BiVO_4$	1.81
CNP	84.32
CNP/B-$BiVO_4$	2.49
WO_3	36.26

Figure 5. UV−vis absorption spectra of $BiVO_4$, WO_3 and CNP/B-$BiVO_4$.

2.6. PEC Degradation Experiments. Degradation of orange II sodium salt was carried out at the fabricated electrodes to evaluate their PEC performance. The oxidation process was performed at an applied anodic potential of 2.0 V. The removal efficiency of the dye was calculated from the following relation:

$$\% \ removal = (A_0 - A_t)/A_0 \times 100$$

where A_0 and A_t are the absorbance values at time $t = 0$ and $t = t$, respectively.

As can be seen in Figure 8a, the CNP/B-$BiVO_4$/WO_3 electrode exhibited the highest degradation efficiency with 92% removal of the dye in 3 h of the PEC process. The performance of the photoanodes follows the order $BiVO_4$ < B-$BiVO_4$ < WO_3 < CNP−$BiVO_4$ < CNP/B-$BiVO_4$ < CNP/B-$BiVO_4$/WO_3. Degradation efficiency at B-doped $BiVO_4$ photoanode is only slightly higher than that obtained at the pristine $BiVO_4$ anode (data not shown). Wang et al. made similar observation in the photocatalytic performance of $BiVO_4$ and B-$BiVO_4$.[53] The authors reported that boron doping narrows the band gap energy of the photocatalyst by a magnitude of 0.04 eV, thus increasing its light absorption in the visible region. It was also suggested that interstitial boron doping can increase the number of oxygen vacancies and V^{4+}, leading to red shifting of the absorption edge and consequently improved photocatalytic performance in the visible light region. It is noteworthy that the performance of pristine $BiVO_4$ is inferior to that of the pure WO_3 nanorods despite the former being a better absorber of visible light. The poor conductivity and low adsorption capability of $BiVO_4$ are some of the factors responsible for its low PEC performance. On the other hand, the relatively large surface area of WO_3 and its excellent conductivity are favorable for the degradation of organic pollutants. However, incorporation of CNP into $BiVO_4$ leads to significant improvement in its PEC performance. In essence, the CNP and B codoped $BiVO_4$ showed much more enhanced performance. Also, incorporation of CNP into the structure of $BiVO_4$ could lead to improved charge transport property and enhanced adsorption capability of the photocatalyst. Apparently, the CNP/B-$BiVO_4$/WO_3 performed best because of the contributions of the various
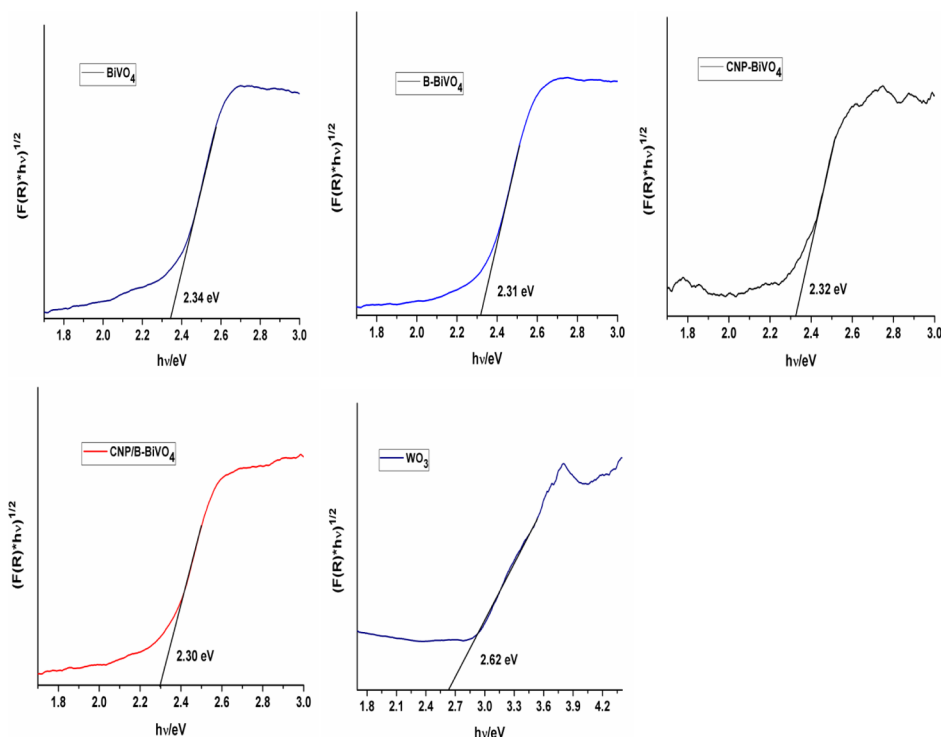
Figure 6. Band gap energies of the catalysts estimated from the plot of Kubelka−Munk function vs incident energy.
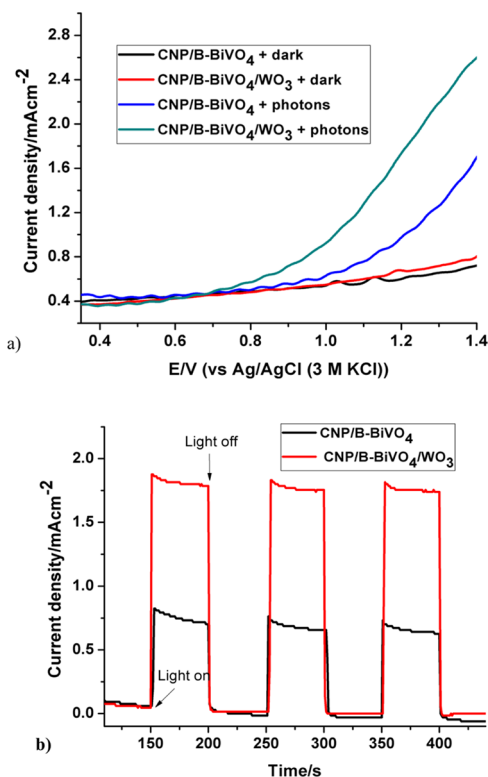

Figure 7. (a) Linear sweep voltammograms of photoanodes measured in 0.1 M Na_2SO_4 and (b) photocurrent response of CNP/B-BiVO$_4$ and CNP/B-BiVO$_4$/WO$_3$ obtained in 5 mg L^{-1} of orange II dye (prepared in 0.1 M Na_2SO_4) at a potential of 1.2 V.

Figure 8. Degradation profiles of orange II sodium salt (a) at different photoanodes (b) by different oxidation processes.

constituent materials. The kinetic rate constants obtained by fitting the degradation experimental data into the Langmuir Hinshelwood kinetic model are 0.0924, 0.1812, 0.254, and 0.845 h^{-1} for BiVO$_4$, WO$_3$, CNP/B-BiVO$_4$, and CNP/B-

BiVO$_4$/WO$_3$, respectively. Figure 8b displays the plots of normalized concentration abatement of the dye via photolysis, electrolysis, and photoelectrocatalysis. It can be seen that the coupled process offers a far more efficient removal of the dye

than the individual processes. This observation further affirms the superiority of PEC oxidation process to both electrochemical oxidation and photocatalytic oxidation processes. The chemical oxygen demand (COD) decay after 3 h of the PEC process at the preferred anode was 58%. For possible practical application, the photoelectrocatalyst ($CNP/B-BiVO_4/WO_3$) was further employed for the degradation of 50 mg L^{-1} (50 mL) of the dye solution under the same experimental conditions. A 56% decolourization was obtained after 3 h of the process.

3. CONCLUSIONS

Two visible-light-sensitive semiconductors, namely, $BiVO_4$ and WO_3, have been synthesized, characterized, and applied for the degradation of a model organic pollutant, orange II dye. $BiVO_4$ was modified with CNP and B to improve its charge transport property and adsorption behavior to increase its PEC efficiency. The kinetic rate constants calculated for the degradation of the contaminants at $BiVO_4$ and WO_3 photoanodes were 0.0924 and 0.1812 h^{-1}, respectively. The much better performance of WO_3 nanorods compared to the undoped $BiVO_4$ may not be unrelated to its morphology, which can retard recombination of photogenerated electron−hole pairs. Doping CNP and B into the structure of $BiVO_4$ led to significant improvement in its PEC performance. Coupling the doped $BiVO_4$ to WO_3 yielded a heterostructured anodic material which showed much more excellent properties than the individual components. The higher performance of this electrode can be linked to the formation of n−n heterojunction, which promotes separation of charges and generation of a large amount of the valence-bound holes, which are needed for the oxidation of the pollutant. This study shows that $BiVO_4$- and WO_3-based anodes have prospects for water remediation via photoelectrocatalysis.

4. EXPERIMENTAL SECTION

4.1. Materials. Sodium tungstate dihydrate ($Na_2WO_4 \cdot 2H_2O$), bismuth nitrate pentahydrate ($Bi(NO_3)_3 \cdot 5H_2O$), sodium metavanadate ($NaVO_3$), sodium chloride ($NaCl$), sodium sulfate (Na_2SO_4), sodium hydrogen carbonate ($NaHCO_3$), sodium hydroxide ($NaOH$), orange II sodium salt, polyethylene glycol (PEG), boric acid (H_3BO_3), and ethanol were purchased from Sigma-Aldrich, South Africa. All solutions were prepared with deionized water.

4.2. Synthesis of WO_3 Nanorods. The synthesis of WO_3 nanorods is as follows: 2.62 g of $Na_2WO_4 \cdot 2H_2O$ was dissolved in 80 mL of deionized water, followed by addition of 1.0 g of NaCl. The homogeneous mixture obtained was then acidified with HCl until the pH was 2.06. Upon addition of HCl, the mixture turned to a white precipitate, and this precursor solution was transferred to a 100 mL Teflon-lined autoclave. The autoclave was sealed and maintained at 180 °C in an oven for 24 h. After cooling to room temperature, the synthesized material was transferred into centrifuge tubes and washed by centrifugation repeatedly with deionized water and then ethanol. The material was then dried at 80 °C in an air oven for 8 h. The powder material obtained after drying was kept for use.

4.3. Preparation of CNPs, $BiVO_4$, and $CNP/B-BiVO_4$. CNPs were prepared from oats purchased from a local market in Johannesburg, South Africa. Oats (5 g) was powdered by grinding. The powder was then put into a crucible and

transferred into a muffle furnace maintained at 400 °C for 2 h. The black material formed was allowed to cool to room temperature, pulverized, and subsequently dispersed in deionized water. The dispersion was centrifuged and the supernatant was decanted into a clean beaker. This process was repeated several times to obtain more supernatants. The water in the supernatant was evaporated and the solid particles left in the beaker were collected and kept for use.

To synthesize pristine $BiVO_4$, 0.61 g of $NaVO_3$ was dissolved in about 40 mL of deionized water and 2.43 g of $Bi(NO_3)_3 \cdot 5H_2O$ were dissolved in 0.1 M HNO_3. The $NaVO_3$ solution was then gradually added to the $Bi(NO_3)_3$ solution. The yellow precursor solution formed was transferred into a Teflon-lined autoclave, sealed, and put into the stainless steel shell. This was then maintained 180 °C for 24 h in an oven. Upon cooling, the material was transferred into centrifuge tubes and washed a few times with water. The yellow substance obtained after decantation was dried in an air oven at 80 °C for 8 h. Preparation of $CNP/B-BiVO_4$ followed the same procedure except that 1.0 g of H_3BO_3 and 10 mg of CNP were added to the solution of $NaVO_3$ prior to mixing with $Bi(NO_3)_3 \cdot 5H_2O$ solution.

4.4. Characterization of the Materials. Powder XRD analysis of the catalysts was done on a Rigaku Smartlab X-ray diffractometer (USA) equipped with Cu kα radiation and operated at 40 kV and 40 mA. The electron images were obtained on a scanning electron microscope (TESCAN, VEGA3 XMU, Czech Republic) and transmission electron microscope (JEOL 2100 HRTEM 200V, Japan). Energy-dispersive X-ray spectrometry analysis was performed on the equipment attached to the scanning electron microscope. DRS was done on a UV−visible spectrophotometer (Shimadzu 2450, Japan), and concentration abatement of the dye was monitored on a UV−visible spectrophotometer (Agilent Cary 60, Malaysia) at its wavelength of maximum absorption. COD was determined on a HACH DR3900 spectrophotometer.

4.5. Fabrication of Electrodes. Ti sheets were first degreased in 40% m/m NaOH solution heated to 80 °C and maintained for 2 h. Etching of the sheets was then carried out in a 18% v/v HCl solution maintained at 98% for 2 h.

The dispersions of $BiVO_4$, $B-BiVO_4$, $CNP/BiVO_4$, $CNP/B-BiVO_4$, and WO_3 were prepared by weighing 0.2 g of each of the catalysts into an ethanolic solution of PEG (containing 2 mL of ethanol and 1 mL of PEG). A mixture of both $CNP/B-BiVO_4$ and WO_3 was also prepared by dispersing 0.1 g of each of the catalysts in an ethanolic solution of PEG. The dispersions were ultrasonicated for 60 min.

The dispersion (100 μL) was drop-cast onto both sides of the prepared Ti sheets with an exposed area of 4 cm^2. The coated sheets were dried in an air oven at a temperature of 250 °C. The coating was repeated once more and the sheets were sintered at 500 °C in a muffle furnace.

4.6. Electrochemical Experiments. Electrochemical measurements were done on a computer-controlled potentiostat (Autolab PGSTAT 302N) using a three-electrode system. The working electrodes used include $BiVO_4/Ti$, $B-BiVO_4/Ti$, $CNP−BiVO_4/Ti$, $CNP/B-BiVO_4/Ti$, WO_3/Ti, and $CNP/B-BiVO_4/WO_3/Ti$, the reference electrode was Ag/AgCl (3 M KCl), and the counter electrode was a coiled platinum wire. Linear sweep voltammetric measurements were carried out in a 0.1 M solution of Na_2SO_4, and amperometric measurements in the presence and absence of photons were performed in 5 mg L^{-1} solution of orange II sodium salt (prepared in 0.1 M

Na_2SO_4). Electrochemical oxidation of the dye was carried out in a quartz photoelectrochemical cell in the presence and absence of light. Typically, 250 mL of the simulated wastewater (containing 5 mg L^{-1} of the analyte) was electrolyzed in an experiment with continuous stirring of the electrolytic solution. The solar light source was an Oriel solar simulator. The simulator has a xenon lamp of 100 W and a UV cutoff filter (Air Mass 1.5 Global filter), giving 1.0 sun output. The distance between the photoelectrochemical cell and the light source was about 5 cm.

■ AUTHOR INFORMATION

Corresponding Author
*E-mail: oarotiba@uj.ac.za. Phone: +27115596200.

ORCID ⊙
Omotayo A. Arotiba: 0000-0002-8227-8684

Notes
The authors declare no competing financial interest.

■ ACKNOWLEDGMENTS

■ REFERENCES

(1) Zhang, X.; Yang, Y.; Ding, S.; Que, W.; Zheng, Z.; Du, Y. Construction of High-Quality $SnO_2@ MoS_2$ Nanohybrids for Promising Photoelectrocatalytic Applications. *Inorg. Chem.* **2017**, *56*, 3386−3393.

(2) Peleyeju, M. G.; Umukoro, E. H.; Tshwenya, L.; Moutloali, R.; Babalola, J. O.; Arotiba, O. A. Photoelectrocatalytic water treatment systems: degradation, kinetics and intermediate products studies of sulfamethoxazole on a TiO_2−exfoliated graphite electrode. *RSC Adv.* **2017**, *7*, 40571−40580.

(3) Peleyeju, M. G.; Arotiba, O. A. Recent trend in visible-light photoelectrocatalytic systems for degradation of organic contaminants in water/wastewater. *Environ. Sci.: Water Res. Technol.* **2018**, *4*, 1389−1411.

(4) Bessegato, G. G.; Cardoso, J. C.; Zanoni, M. V. B. Enhanced photoelectrocatalytic degradation of an acid dye with boron-doped TiO_2 nanotube anodes. *Catal. Today* **2015**, *240*, 100−106.

(5) Deng, W.; Zhao, H.; Pan, F.; Feng, X.; Jung, B.; Abdel-Wahab, A.; Batchelor, B.; Li, Y. Visible-light-driven photocatalytic degradation of organic water pollutants promoted by sulfite addition. *Environ. Sci. Technol.* **2017**, *51*, 13372−13379.

(6) Rincón, N. C.; Hammouda, S. B.; Sillanpää, M.; Barrios, V. E. Enhanced photocatalytic performance of zinc oxide nanostructures via photoirradiation hybridisation with graphene oxide for the degradation of triclosan under visible light: Synthesis, characterisation and mechanistic study. *J. Environ. Chem. Eng.* **2018**, *6*, 6554−6567.

(7) Ma, R.; Zhang, S.; Li, L.; Gu, P.; Wen, T.; Khan, A.; Li, S.; Li, B.; Wang, S.; Wang, X. Enhanced Visible-Light-Induced Photoactivity of Type-II $CeO_2/g-C_3N_4$ Nanosheet toward Organic Pollutants Degradation. *ACS Sustainable Chem. Eng.* **2019**, *7*, 9699−9708.

(8) Monfort, O.; Pop, L.-C.; Sfaelou, S.; Plecenik, T.; Roch, T.; Dracopoulos, V.; Stathatos, E.; Plesch, G.; Lianos, P. Photoelectrocatalytic hydrogen production by water splitting using $BiVO_4$ photoanodes. *Chem. Eng. J.* **2016**, *286*, 91−97.

(9) Zhou, Y.; Zhang, L.; Lin, L.; Wygant, B. R.; Liu, Y.; Zhu, Y.; Zheng, Y.; Mullins, C. B.; Zhao, Y.; Zhang, X.; Yu, G. Highly efficient photoelectrochemical water splitting from hierarchical $WO_3/BiVO_4$ nanoporous sphere arrays. *Nano Lett.* **2017**, *17*, 8012−8017.

(10) Monfort, O.; Raptis, D.; Satrapinskyy, L.; Roch, T.; Plesch, G.; Lianos, P. Production of hydrogen by water splitting in a photoelectrochemical cell using a $BiVO_4/TiO_2$ layered photoanode. *Electrochim. Acta* **2017**, *251*, 244−249.

(11) Tolod, K.; Hernández, S.; Russo, N. Recent advances in the $BiVO_4$ photocatalyst for sun-driven water oxidation: top-performing photoanodes and scale-up challenges. *Catalysts* **2017**, *7*, 13.

(12) Monfort, O.; Sfaelou, S.; Satrapinskyy, L.; Plecenik, T.; Roch, T.; Plesch, G.; Lianos, P. Comparative study between pristine and Nb-modified $BiVO_4$ films employed for photoelectrocatalytic production of H_2 by water splitting and for photocatalytic degradation of organic pollutants under simulated solar light. *Catal. Today* **2017**, *280*, 51−57.

(13) Ahmed, T.; Zhang, H.-l.; Xu, H.-b.; Zhang, Y. m-BiVO4 hollow spheres coated on carbon fiber with superior reusability as photocatalyst. *Colloids Surf., A* **2017**, *531*, 213−220.

(14) Malathi, A.; Vasanthakumar, V.; Arunachalam, P.; Madhavan, J.; Ghanem, M. A. A low cost additive-free facile synthesis of $BiFeWO_6/BiVO_4$ nanocomposite with enhanced visible-light induced photocatalytic activity. *J. Colloid Interface Sci.* **2017**, *506*, 553−563.

(15) He, Z.; Shi, Y.; Gao, C.; Wen, L.; Chen, J.; Song, S. BiOCl/ $BiVO_4$ p−n heterojunction with enhanced photocatalytic activity under visible-light irradiation. *J. Phys. Chem. C* **2014**, *118*, 389−398.

(16) Sun, Y.; Qu, B.; Liu, Q.; Gao, S.; Yan, Z.; Yan, W.; Pan, B.; Wei, S.; Xie, Y. Highly efficient visible-light-driven photocatalytic activities in synthetic ordered monoclinic $BiVO_4$ quantum tubes−graphene nanocomposites. *Nanoscale* **2012**, *4*, 3761−3767.

(17) Shang, M.; Wang, W.; Sun, S.; Ren, J.; Zhou, L.; Zhang, L. Efficient visible light-induced photocatalytic degradation of contaminant by spindle-like PANI/BiVO4. *J. Phys. Chem. C* **2009**, *113*, 20228−20233.

(18) Geng, Y.; Zhang, P.; Li, N.; Sun, Z. Synthesis of Co doped $BiVO_4$ with enhanced visible-light photocatalytic activities. *J. Alloys Compd.* **2015**, *651*, 744−748.

(19) Sun, J.; Guo, Y.; Wang, Y.; Cao, D.; Tian, S.; Xiao, K.; Mao, R.; Zhao, X. H_2O_2 assisted photoelectrocatalytic degradation of diclofenac sodium at $gC_3N_4/BiVO_4$ photoanode under visible light irradiation. *Chem. Eng. J.* **2018**, *332*, 312−320.

(20) Dong, P.; Hou, G.; Xi, X.; Shao, R.; Dong, F. WO 3-based photocatalysts: morphology control, activity enhancement and multifunctional applications. *Environ. Sci.: Nano* **2017**, *4*, 539−557.

(21) Sfaelou, S.; Pop, L.-C.; Monfort, O.; Dracopoulos, V.; Lianos, P. Mesoporous WO_3 photoanodes for hydrogen production by water splitting and PhotoFuelCell operation. *Int. J. Hydrogen Energy* **2016**, *41*, 5902−5907.

(22) Hilliard, S.; Baldinozzi, G.; Friedrich, D.; Kressman, S.; Strub, H.; Artero, V.; Laberty-Robert, C. Mesoporous thin film WO_3 photoanode for photoelectrochemical water splitting: a sol−gel dip coating approach. *Sustainable Energy Fuels* **2017**, *1*, 145−153.

(23) Weng, B.; Wu, J.; Zhang, N.; Xu, Y.-J. Observing the role of graphene in boosting the two-electron reduction of oxygen in graphene−WO3 nanorod photocatalysts. *Langmuir* **2014**, *30*, 5574−5584.

(24) Sakai, Y.; Shimanaka, A.; Shioi, M.; Kato, S.; Satokawa, S.; Kojima, T.; Yamasaki, A. Fabrication of high-sensitivity palladium loaded tungsten trioxide photocatalyst by photodeposite method. *Catal. Today* **2015**, *241*, 2−7.

(25) Huang, Z.-F.; Song, J.; Pan, L.; Zhang, X.; Wang, L.; Zou, J.-J. Tungsten oxides for photocatalysis, electrochemistry, and phototherapy. *Adv. Mater.* **2015**, *27*, 5309−5327.

(26) Zhang, T.; Su, J.; Guo, L. Morphology engineering of WO 3/ BiVO 4 heterojunctions for efficient photocatalytic water oxidation. *CrystEngComm* **2016**, *18*, 8961−8970.

(27) Dirany, N.; Arab, M.; Leroux, C.; Villain, S.; Madigou, V.; Gavarri, J. R. Effect of WO3 nanoparticles morphology on the catalytic properties. *Mater. Today: Proc.* **2016**, *3*, 230−234.

(28) Ahmed, B.; Kumar, S.; Ojha, A. K.; Donfack, P.; Materny, A. Facile and controlled synthesis of aligned WO_3 nanorods and nanosheets as an efficient photocatalyst material. *Spectrochim. Acta, Part A* **2017**, *175*, 250−261.

(29) Theerthagiri, J.; Senthil, R. A.; Malathi, A.; Selvi, A.; Madhavan, J.; Ashokkumar, M. Synthesis and characterization of a CuS−WO 3 composite photocatalyst for enhanced visible light photocatalytic activity. *RSC Adv.* **2015**, *5*, 52718−52725.

(30) Zhang, J.; Ma, Y.; Du, Y.; Jiang, H.; Zhou, D.; Dong, S. Carbon nanodots/WO_3 nanorods Z-scheme composites: Remarkably enhanced photocatalytic performance under broad spectrum. *Appl. Catal., B* **2017**, *209*, 253−264.

(31) Yao, S.; Qu, F.; Wang, G.; Wu, X. Facile hydrothermal synthesis of WO_3 nanorods for photocatalysts and supercapacitors. *J. Alloys Compd.* **2017**, *724*, 695−702.

(32) Xia, L.; Bai, J.; Li, J.; Zeng, Q.; Li, X.; Zhou, B. A highly efficient $BiVO_4$/WO_3/W heterojunction photoanode for visible-light responsive dual photoelectrode photocatalytic fuel cell. *Appl. Catal., B* **2016**, *183*, 224−230.

(33) Ho-Kimura, S.; Moniz, S. J. A.; Handoko, A. D.; Tang, J. Enhanced photoelectrochemical water splitting by nanostructured $BiVO_4$−TiO_2 composite electrodes. *J. Mater. Chem. A* **2014**, *2*, 3948−3953.

(34) Kim, E. S.; Kang, H. J.; Magesh, G.; Kim, J. Y.; Jang, J.-W.; Lee, J. S. Improved photoelectrochemical activity of $CaFe2O_4$/$BiVO_4$ heterojunction photoanode by reduced surface recombination in solar water oxidation. *ACS Appl. Mater. Interfaces* **2014**, *6*, 17762−17769.

(35) Wang, S.; Yun, J.-H.; Luo, B.; Butburee, T.; Peerakiatkhajohn, P.; Thaweesak, S.; Xiao, M.; Wang, L. Recent progress on visible light responsive heterojunctions for photocatalytic applications. *J. Mater. Sci. Technol.* **2017**, *33*, 1−22.

(36) Yuan, Y.-J.; Wang, F.; Hu, B.; Lu, H.-W.; Yu, Z.-T.; Zou, Z.-G. Significant enhancement in photocatalytic hydrogen evolution from water using a MoS 2 nanosheet-coated ZnO heterostructure photocatalyst. *Dalton Trans.* **2015**, *44*, 10997−11003.

(37) Xia, L.; Bai, J.; Li, J.; Zeng, Q.; Li, L.; Zhou, B. High-performance $BiVO_4$ photoanodes cocatalyzed with an ultrathin α-Fe_2O_3 layer for photoelectrochemical application. *Appl. Catal., B* **2017**, *204*, 127−133.

(38) Martins, A. S.; Nuñez, L.; Lanza, M. R. d. V. Enhanced photoelectrocatalytic performance of TiO_2 nanotube array modified with WO_3 applied to the degradation of the endocrine disruptor propyl paraben. *J. Electroanal. Chem.* **2017**, *802*, 33−39.

(39) Wei, Z.; Liang, F.; Liu, Y.; Luo, W.; Wang, J.; Yao, W.; Zhu, Y. Photoelectrocatalytic degradation of phenol-containing wastewater by TiO_2/gC_3N_4 hybrid heterostructure thin film. *Appl. Catal., B* **2017**, *201*, 600−606.

(40) Zeng, Q.; Li, J.; Li, L.; Bai, J.; Xia, L.; Zhou, B. Synthesis of WO_3/$BiVO_4$ photoanode using a reaction of bismuth nitrate with peroxovanadate on WO_3 film for efficient photoelectrocatalytic water splitting and organic pollutant degradation. *Appl. Catal., B* **2017**, *217*, 21−29.

(41) Chatchai, P.; Nosaka, A. Y.; Nosaka, Y. Photoelectrocatalytic performance of WO_3/$BiVO_4$ toward the dye degradation. *Electrochim. Acta* **2013**, *94*, 314−319.

(42) Liu, Y.; Huang, B.; Dai, Y.; Zhang, X.; Qin, X.; Jiang, M.; Whangbo, M.-H. Selective ethanol formation from photocatalytic reduction of carbon dioxide in water with $BiVO_4$ photocatalyst. *Catal. Commun.* **2009**, *11*, 210−213.

(43) Yan, Y.; Sun, S.; Song, Y.; Yan, X.; Guan, W.; Liu, X.; Shi, W. Microwave-assisted in situ synthesis of reduced graphene oxide-$BiVO_4$ composite photocatalysts and their enhanced photocatalytic performance for the degradation of ciprofloxacin. *J. Hazard. Mater.* **2013**, *250−251*, 106−114.

(44) Adhikari, S.; Sarkar, D. High efficient electrochromic WO_3 nanofibers. *Electrochim. Acta* **2014**, *138*, 115−123.

(45) Zhang, L. J.; Li, S.; Liu, B. K.; Wang, D. J.; Xie, T. F. Highly efficient CdS/WO_3 photocatalysts: Z-scheme photocatalytic mecha-

nism for their enhanced photocatalytic H_2 evolution under visible light. *ACS Catal.* **2014**, *4*, 3724−3729.

(46) Luo, J.; Zhou, X.; Ma, L.; Xu, X. Enhanced visible-light-driven photocatalytic activity of WO_3/BiOI heterojunction photocatalysts. *J. Mol. Catal. A: Chem.* **2015**, *410*, 168−176.

(47) Cui, L.; Ding, X.; Wang, Y.; Shi, H.; Huang, L.; Zuo, Y.; Kang, S. Facile preparation of Z-scheme WO_3/gC_3N_4 composite photocatalyst with enhanced photocatalytic performance under visible light. *Appl. Surf. Sci.* **2017**, *391*, 202−210.

(48) Li, F.; Zhang, L.; Chen, X.; Liu, Y. L.; Xu, S. G.; Cao, S. K. Synergistically enhanced photocatalytic reduction of CO_2 on N−Fe codoped $BiVO_4$ under visible light irradiation. *Phys. Chem. Chem. Phys.* **2017**, *19*, 21862−21868.

(49) Chen, L.; Meng, D.; Wu, X.; Wang, A.; Wang, J.; Wang, Y.; Yu, M. In situ synthesis of V4+ and Ce3+ self-doped $BiVO_4$/CeO_2 heterostructured nanocomposites with high surface areas and enhanced visible-light photocatalytic activity. *J. Phys. Chem. C* **2016**, *120*, 18548−18559.

(50) Zheng, J. Y.; Song, G.; Hong, J.; Van, T. K.; Pawar, A. U.; Kim, D. Y.; Kim, C. W.; Haider, Z.; Kang, Y. S. Facile fabrication of WO3 nanoplates thin films with dominant crystal facet of (002) for water splitting. *Cryst. Growth Des.* **2014**, *14*, 6057−6066.

(51) Hong, S. J.; Lee, S.; Jang, J. S.; Lee, J. S. Heterojunction $BiVO_4$/WO_3 electrodes for enhanced photoactivity of water oxidation. *Energy Environ. Sci.* **2011**, *4*, 1781−1787.

(52) Lee, M. G.; Kim, D. H.; Sohn, W.; Moon, C. W.; Park, H.; Lee, S.; Jang, H. W. Conformally coated $BiVO_4$ nanodots on porosity-controlled WO_3 nanorods as highly efficient type II heterojunction photoanodes for water oxidation. *Nano Energy* **2016**, *28*, 250−260.

(53) Wang, M.; Che, Y.; Niu, C.; Dang, M.; Dong, D. Effective visible light-active boron and europium co-doped $BiVO_4$ synthesized by sol−gel method for photodegradion of methyl orange. *J. Hazard. Mater.* **2013**, *262*, 447−455.